

# Effect of the flow composition on outflow rates from accretion discs around black holes

Rajiv Kumar<sup>1</sup>, Chandra B. Singh<sup>2</sup>, Indranil Chattopadhyay<sup>1</sup>, Sandip K. Chakrabarti<sup>3,2</sup>

<sup>1</sup>*Aryabhata Research Institute of Observational Sciences (ARIES), Manora Peak, Nainital-263002, India*

<sup>2</sup>*Indian Centre for Space Physics, Chalanika 43, Garia Station Rd., Kolkata, 700084, India*

<sup>3</sup>*S.N. Bose National Centre for Basic Sciences, Salt Lake, Kolkata 700098, India*

## ABSTRACT

We studied the outflow behaviour from accretion discs around black holes taking into account the vertical equilibrium accretion flow model. The outflow rate is found to depend crucially on flow composition. Our approach is to study the outflow behaviour as function of inflow around black holes with an equation of state which allows flow to be thermally relativistic close to black holes and non relativistic far away from black holes. We studied shock ejection model. A pure electron positron pair flow never undergoes shock transition while presence of some baryons (common in outflows and jets) makes it possible to have standing shock waves in the flow. It can be concluded that the presence of protons is necessary for the flow to show the outflow behaviour. The outflow rate is maximum when the flow contains the proton number density which is 27% of the electron number density. We conclude that a pure electron-positron jet is unlikely to form.

**Key words:** hydrodynamics, black hole physics, accretion, accretion discs, jets and outflows

## 1 INTRODUCTION

One of the spectacular phenomena associated with many classes of astrophysical objects is the formation of outflows and jets. Systems which have been associated with winds and jets are active galactic nuclei (AGNs e.g., M87), young stellar objects (YSOs e.g., HH 30, HH 34), high mass X-ray binaries (HMXB e.g., SS433, Cyg X-3), black hole X-ray transients (e.g., GRS 1915+105, GRO 1655-40) and low mass X-ray binaries (LMXB e.g., Cir X-1). In

most of the cases like YSOs, X-ray binaries and AGNs, the accretion disc is associated with the production of outflows and jets. In case of YSOs, such as HH 30 (Burrows 1996), the disc-jet connection has been established. In case of black hole candidates like microquasars and AGNs, jets have to originate from the accretion disc, since black holes do not have any atmosphere or hard surface. What is even more intriguing, is that the entire accretion disc does not seem to participate in the generation of the outflow or jet. VLBI observations of M87 (Junor et. al. 1999) have shown that the jet originates from the immediate vicinity ( $\sim 50r_g$ ) of a black hole. Moreover, recent detailed observations of various microquasars also show, that the jet states are strongly correlated with the spectral states of the associated accretion disc (Gallo et. al. 2003; Fender *et al.* 2010; Rushton *et al.* 2010). So the physics of accretion disc is crucial to understand how the jets are launched.

The thin disc, also known as the Shakura-Sunyaev  $\alpha$  disc (SS disc) or ‘standard’ disc, was the first successful disc model to explain the thermal component of the spectra coming from the black hole candidates (Shakura & Sunyaev 1973; Novikov & Thorne 1973). However, the inner boundary of the disc was *ad hoc*, and the SS disc was unable to explain the hard non-thermal part of the spectra. Since the inner boundary condition around a black hole is necessarily transonic, models with significant advection gained popularity, and since discs with advection tends to be hotter, it became a candidate to explain high energy radiations. Out of all the disc models in the advective domain, ADAF (advection dominated accretion flow) gained overwhelming popularity (Narayan *et al.* 1997), and is a model characterized by a flow which is mostly subsonic and radiatively inefficient. However, it has been shown earlier, that more than one sonic point may exist for inviscid advective flow (Liang & Thompson, 1980; Chakrabarti, 1989), and was later confirmed for viscous flow too (Chakrabarti 1990, 1996; Lu *et al.* 1999; Chakrabarti & Das 2004; Becker *et al.* 2008). It was also shown that, the ADAF type solutions are a subset of the general advective solutions (Chakrabarti 1996; Lu *et al.* 1999; Becker *et al.* 2008; Kumar & Chattopadhyay 2013). Interestingly enough, in the multiple critical (or sonic) point *i.e.*, MCP domain of the energy-angular momentum parameter space, matter passing through the outer sonic point may undergo centrifugal barrier induced shock transition (Fukue 1987; Chakrabarti 1989, 1996; Becker *et al.* 2008; Kumar & Chattopadhyay 2013). A shocked accretion disc solution has various advantages. Numerical simulations established that, the unbalanced thermal gradient term along the vertical direction in the post-shock region of the disc, drives bipolar outflows (Molteni *et al.* 1994, 1996). In a model solution starting with sub-Keplerian (advective) and Keplerian

matter, Chakrabarti & Titarchuk (1995) showed that the soft, hard and the intermediate spectral states can be satisfactorily explained. The post-shock disc inverse-Comptonizes the intercepted soft photons to produce the hard power-law tail and produces the so-called hard spectral state, while absence of or weakened post-shock disc produces essentially the soft spectral state. These assertions are vindicated by observations (Smith *et al.* 2001, 2002, 2007), and also by numerical simulations (Giri & Chakrabarti 2013). Moreover, oscillating and transient shocks explain the low-frequency quasi periodic oscillation (QPO) and its evolution during spectral state transitions (Nandi *et al.* 2012).

Various outflow models exist in the literature (Blandford & Payne 1982; Punsly & Coroniti 1990; Chattopadhyay 2005) which concentrate on collimation and acceleration of outflows. However, very few addressed the most important issue of the outflow rate as a function of the inflow parameters. Chakrabarti (1999) attempted to estimate the outflow rate by considering simple hydrodynamical equations such as those applicable to conical inflows and outflows. The work of Chakrabarti (1999) was later extended to rotating inviscid flows (Das *et al.* 2001; Singh & Chakrabarti 2011a,b, 2012), as well as the viscid flows (Chattopadhyay & Das 2007; Das & Chattopadhyay 2008; Kumar & Chattopadhyay 2013).

Majority of these works mentioned above, however, used a constant polytropic index and did not consider the variation of it from a large distance to the black hole and from the disc phase to the jet phase. Realistically, at large distances away from the central object, matter should be cold, but as it dives into the central object its thermal and kinetic energy increases. A flow with an equation of state described by a fixed  $\Gamma$  (adiabatic index) need not describe the behaviour of accreting matter properly from infinity to the horizon, because for ultra-relativistic non-degenerate gas  $\Gamma = 4/3$ , and that for non-relativistic one, it is  $\Gamma = 5/3$ .  $\Gamma$  takes intermediate values for trans-relativistic thermal energy. The equation of state (hereafter, EoS) of a single species relativistic gas was computed by Chandrasekhar (1938); Synge (1957), which gave the correct description of the flow in all temperature range, and we call the EoS as RP (relativistically perfect). However, RP is a combination of modified Bessel's functions and which makes its usage non-trivial and fairly expensive from computational point of view. Hence many workers proposed approximate EoS for single species flow, which are close to RP and yet easy to use (Taub 1948; Mathews 1971; Ryu *et al.* 2006). For the very first time Blumenthal & Mathews (1976, hereafter BM76), used the EoS of Mathews (1971) and solved for radial accretion in general relativity. Following the suggestions of BM76, Chattopadhyay (2008); Chattopadhyay & Ryu (2009) pro-

posed an EoS of multi-species flow composed of electrons, protons and positrons, although EoS for electron-proton flow was suggested earlier (Fukue 1987). Chattopadhyay (2008); Chattopadhyay & Ryu (2009) showed in a general relativistic investigation that, a purely electron-positron adiabatic flow is the slowest, thermally least relativistic flow, compared to flows containing protons and leptons, and consequently, electron-positron flows do not show accretion shocks (Chattopadhyay 2008; Chattopadhyay & Chakrabarti 2011). It was also shown that electron-proton (*i.e.*, equal number of electrons & protons) flow is not the most relativistic case. However, when the proton number density is  $\sim 20\%$  of the electron number density, the flow becomes most relativistic. Therefore, an estimation of the outflow rate from the inflow parameters using an equation of state of a fully ionized flow would be an important contribution. In this paper, we precisely do this. The plan of our paper is the following: in the next Section, we present the assumptions and equations governing inflow and outflow from accretion discs around black holes. In Section 3, we present a detailed analysis of critical point behaviour and solution of accreting flow. We then present our results exhibiting the dependence of outflow rates on flow composition, energy and angular momentum of the accretion disc. Finally, in Section 4, we carry out discussion and make concluding remarks.

## 2 ASSUMPTIONS AND EQUATIONS

We consider a fully ionized, adiabatic, rotating and accreting axisymmetric disc around a Schwarzschild black hole. For mathematical simplicity, space-time around the black hole is described by the Paczyński-Wiita (hereafter PW) pseudo-Newtonian potential (Paczyński & Wiita 1980). We have used PW potential in order to simplify our calculations while retaining all the essential qualitative features of strong gravity. Moreover, it is easier to incorporate more complicated physics in pseudo-Newtonian scheme. Earlier investigations of disc-jet system had been to employ general relativity and fixed  $\Gamma$  EoS, or general relativity with relativistic EoS, or PW approach with fixed  $\Gamma$  EoS. So far, the approach with PW potential which is coupled with a variable  $\Gamma$  EoS was not attempted and ours is the first to do so.

## 2.1 Equation of state

Following Chattopadhyay (2008); Chattopadhyay & Ryu (2009), we consider flows which are composed of electrons ( $e^-$ ), positrons ( $e^+$ ) and protons ( $p^+$ ) of varying proportions, but always maintaining the overall charge neutrality. The number density is given by,

$$n = \Sigma_i n_i = n_{e^-} + n_{e^+} + n_{p^+}, \quad (1)$$

where,  $n_{e^-}$ ,  $n_{e^+}$  and  $n_{p^+}$  are the electron, positron and proton number densities, respectively. Charge neutrality condition over a reasonable volume element demands that

$$n_{e^-} = n_{e^+} + n_{p^+}, \quad (2)$$

which implies,

$$n = 2n_{e^-}, \text{ and } n_{e^+} = n_{e^-}(1 - \xi), \quad (3)$$

where  $\xi = n_{p^+}/n_{e^-}$  is the relative proportion of protons. The mass density is given by

$$\rho = \Sigma_i n_i m_i = n_{e^-} m_{e^-} [2 - \xi(1 - 1/\eta)], \quad (4)$$

where,  $\eta = m_{e^-}/m_{p^+}$ , and  $m_{e^-}$  and  $m_{p^+}$  are the electron and proton masses, respectively. For single temperature flows, the isotropic pressure is given by

$$p = \Sigma_i p_i = 2n_{e^-} kT = 2n_{e^-} m_{e^-} c^2 \Theta. \quad (5)$$

The EoS for multi-species flow is (Chattopadhyay 2008; Chattopadhyay & Ryu 2009)

$$\bar{e} = \Sigma_i e_i = \Sigma \left[ n_i m_i c^2 + p_i \left( \frac{9p_i + 3n_i m_i c^2}{3p_i + 2n_i m_i c^2} \right) \right]. \quad (6)$$

The non-dimensional temperature is defined with respect to the electron rest mass energy,  $\Theta = kT/(m_{e^-} c^2)$ . Using equations (1)-(5), the expression of the energy density in equation (6) simplifies to,

$$\bar{e} = n_{e^-} m_{e^-} c^2 f = \rho_{e^-} c^2 f = \frac{\rho c^2 f}{[2 - \xi(1 - 1/\eta)]}, \quad (7)$$

where,

$$f = (2 - \xi) \left[ 1 + \Theta \left( \frac{9\Theta + 3}{3\Theta + 2} \right) \right] + \xi \left[ \frac{1}{\eta} + \Theta \left( \frac{9\Theta + 3/\eta}{3\Theta + 2/\eta} \right) \right].$$

The enthalpy is given by,

$$h = \frac{(\bar{e} + p)}{\rho} = \frac{f c^2}{K} + \frac{2c^2 \Theta}{K}, \quad (8)$$

where,  $K = [2 - \xi(1 - 1/\eta)]$ .

The expression of the polytropic index is given by,

$$N = \frac{1}{2} \frac{df}{d\Theta}. \quad (9)$$

The adiabatic index is

$$\Gamma = 1 + \frac{1}{N}. \quad (10)$$

## 2.2 Equations of motion

The length, time and velocity scales are measured in units of  $r_g = 2GM_{BH}/c^2$ ,  $r_g/c = 2GM_{BH}/c^3$  and  $c$ , respectively, where,  $r_g$  is the Schwarzschild radius,  $M_{BH}$  is the mass of the black hole,  $G$  is the gravitational constant, and  $c$  is the velocity of light, this amounts to  $2G = M_{BH} = c = 1$ . Hereafter, all equations are written using the above unit system. It is to be noted though, we have retained the same symbols for the thermodynamic quantities like  $\rho$ ,  $p$  etc, in the dimensionless form too.

### 2.2.1 Inflow

In our study we neglect the non-conservative processes and magnetic fields. We consider the steady and radial flow assumptions.

In this case, the radial momentum equation is given by,

$$\vartheta \frac{d\vartheta}{dx} + \frac{1}{\rho} \frac{dp}{dx} - \frac{\lambda^2}{x^3} + \frac{1}{2(x-1)^2} = 0. \quad (11)$$

Here,  $\lambda$ ,  $\vartheta$ , and  $x$  are the specific angular momentum, the infall velocity, and the radial coordinate in the units described above. The integral form of the eq.(11) gives the Bernoulli parameter and is written as

$$\mathcal{E} = \frac{\vartheta^2}{2} + h + \frac{\lambda^2}{2x^2} - \frac{1}{2(x-1)} \quad (12)$$

and is also called as specific energy of the flow.

The mass conservation equation is given by,

$$\dot{M}_{in} = 2\pi\Sigma\vartheta x, \quad (13)$$

where  $\Sigma = 2\rho H$  is the vertically integrated surface density of the flow.

The disc matter is in hydrostatic equilibrium in the vertical direction, and the half height is given by (Chakrabarti 1989)

$$H = 2\sqrt{\frac{\Theta x}{K}}(x-1). \quad (14)$$

The entropy generation equation or the first law of thermodynamics is given by,

$$\frac{de}{dx} - \frac{p}{\rho^2} \frac{d\rho}{dx} = 0, \quad (15)$$

here,  $e = \bar{e}/\rho = f/K$ , where  $c = 1$ . Integrating eq.(15), and using the definition of  $e$ ,  $\rho$  (eq. 4), and  $p$  (eq. 5), we get

$$\rho = \mathcal{K} \exp(k_3) \Theta^{3/2} (3\Theta + 2)^{k_1} (3\Theta + 2/\eta)^{k_2}, \quad (16)$$

where,  $k_1 = 3(2 - \xi)/4$ ,  $k_2 = 3\xi/4$ , and  $k_3 = (f - K)/(2\Theta)$ . This is the adiabatic equation of state for multispecies flows and  $\mathcal{K}$  is the constant of entropy. Using equations (13) and (16), we can define entropy accretion rate ( $\dot{\mathcal{M}}$ ) as

$$\dot{\mathcal{M}} = \frac{\dot{M}_{in}}{4\pi\mathcal{K}} = \vartheta Hx \exp(k_3) \Theta^{3/2} (3\Theta + 2)^{k_1} (3\Theta + 2/\eta)^{k_2}, \quad (17)$$

here,  $\dot{\mathcal{M}}$  is also constant for inviscid multispecies relativistic flows.

Using equations (13) and (14) in equation (15), we get

$$\frac{d\Theta}{dx} = -\frac{2\Theta}{2N+1} \left[ \frac{1}{\vartheta} \frac{d\vartheta}{dx} + \frac{5x-3}{2x(x-1)} \right]. \quad (18)$$

Using equations (8) and (18) in equation (11), we get

$$\frac{d\vartheta}{dx} = \frac{a^2 \left[ \frac{2N}{2N+1} \frac{5x-3}{2x(x-1)} \right] + \frac{\lambda^2}{x^3} - \frac{1}{2(x-1)^2}}{\vartheta - \frac{a^2}{\vartheta} \left[ \frac{2N}{2N+1} \right]}, \quad (19)$$

where,  $a$  is the adiabatic sound speed given by,  $a^2 = 2\Theta\Gamma/K$ .

### 2.2.2 Critical-point conditions

Gravity, by the very act of pulling matter towards the gravitating centre, primarily causes the increase of the infall speed of the matter, but as a secondary effect, also compresses the in flowing matter and thereby increasing its temperature, and consequently, the sound speed. This causes the flow velocity to cross the local sound speed at a finite distance, which is termed as the sonic point or the critical point of the flow. If the matter is rotating, then the centrifugal force opposes the effect of gravity. Since the centrifugal force is  $\propto x^{-3}$  and is axisymmetric, it breaks the spherical symmetry of gravity, causing the formation of multiple sonic points in a significant range of  $\mathcal{E} - \lambda$  parameter space (Liang & Thompson 1980; Chakrabarti 1989). At the sonic point  $d\vartheta/dx \rightarrow 0/0$ , which gives us the critical or sonic point conditions,

$$a_c^2 = (\Gamma_c + 1) \left( \frac{5x_c - 3}{x_c(x_c - 1)} \right) \left( \frac{1}{2(x_c - 1)^2} - \frac{\lambda_c^2}{x_c^3} \right), \quad (20)$$

and

$$\vartheta_c = \sqrt{\frac{2}{\Gamma_c + 1}} a_c. \quad (21)$$

The subscript  $c$  denotes the quantities at the critical point during accretion flow. At a critical point,  $d\vartheta/dx$  is obtained by using the l'Hospital rule,

$$\left(\frac{d\vartheta}{dx}\right)_{x_c} = \frac{(d\mathcal{N}/dx)_{x_c}}{(d\mathcal{D}/dx)_{x_c}}, \quad (22)$$

where,  $\mathcal{N}$  and  $\mathcal{D}$  are the numerator and denominator of equation (19). The equation becomes,

$$A \left(\frac{d\vartheta}{dx}\right)_{x_c}^2 + B \left(\frac{d\vartheta}{dx}\right)_{x_c} + C = 0, \quad (23)$$

where,

$$A = 2 \left[ 1 + \frac{C_p}{\Gamma_c(2N_c + 1)} \right],$$

$$B = \frac{2\vartheta_c C_p (5x_c - 3)}{\Gamma_c(2N_c + 1)x_c(x_c - 1)},$$

$$C = \frac{\vartheta_c^2 C_p (5x_c - 3)^2}{2\Gamma_c(2N_c + 1)x_c^2(x_c - 1)^2} + \frac{\vartheta_c^2(5x_c^2 - 6x_c + 3)}{(2x_c^2(x_c - 1)^2)} + \frac{3\lambda_c^2}{x_c^4} - \frac{1}{(x_c - 1)^3}$$

and

$$C_p = \Gamma_c + \frac{\Theta_c}{\Gamma_c + 1} (d\Gamma/d\Theta)_c.$$

Since eq.(23) has two roots, they may be either real or complex conjugates depending on the discriminant  $D_r = B^2 - 4AC$  of this equation. This also gives the nature of the critical points. If  $D_r < 0$  then the critical point will be spiral or  $O-$  type and if  $D_r > 0$  then it will either be saddle type (*i.e.*,  $X$  type if  $C/A < 0$ ), or nodal type (if  $C/A > 0$ ). Depending on the relative strengths of thermal energy and rotational energy of the flow, the accreting flow may have one to three sonic points. Out of the possible three sonic points, only two are physical (in the sense, the flow actually passes through them)  $X$ -type and one is unphysical  $O$ -type which forms in between the two  $X$ -type sonic points. The sonic point which forms closer to the horizon is called the inner sonic point ( $x_{ci}$ ), and the one far away is called outer sonic point ( $x_{co}$ ). For flows with very low angular momentum or  $\lambda$ , generally only  $x_{co}$  forms, and flows with very high  $\lambda$  only  $x_{ci}$  forms, but for intermediate  $\lambda$ , multiple sonic may form (Liang & Thompson 1980; Fukue 1987; Chakrabarti 1989; Chattopadhyay & Chakrabarti 2011; Kumar & Chattopadhyay 2013).



### 2.2.3 Shock conditions

In the domain of multiple sonic points, supersonic matter through outer sonic point, may be slowed down due to the centrifugal barrier at  $x \lesssim \text{few} \times 10 r_g$ . If the barrier is strong enough it may produce a centrifugal barrier mediated shock transition. In presence of mass loss, the mass and the momentum flux condition across the shock is given by (Chattopadhyay & Das 2007; Kumar & Chattopadhyay 2013),

$$\dot{M}_+ = \dot{M}_-(1 - R_{\dot{m}}), \quad (24)$$

and,

$$W_+ + \Sigma_+ \vartheta_+^2 = W_- + \Sigma_- \vartheta_-^2. \quad (25)$$

Here, subscripts minus (-) and plus (+) denote the quantities of subsonic and supersonic branch of the accretion flows, respectively, and, if the mass outflow rate is  $\dot{M}_{out}$ , then the relative mass outflow rate is  $R_{\dot{m}} = \dot{M}_{out}/\dot{M}_-$ . Moreover,  $W = 2pH$  is the vertically integrated thermal pressure. The third condition will define the type of shock. If there is no energy loss at the shock front, then we have an adiabatic shock.

$$\mathcal{E}_+ = \mathcal{E}_-. \quad (26)$$

If there is some energy exchange, it becomes a dissipative shock. In this case,

$$\mathcal{E}_+ = \mathcal{E}_- - \Delta\mathcal{E}, \text{ where, } \Delta\mathcal{E} = f_e(h_+ - h_-), \quad (27)$$

here,  $f_e$  is the dissipation parameter. If the entropy is conserved across the shock front, then it is called an isentropic shock, and is given by,

$$\mathcal{K}_+ = \mathcal{K}_-. \quad (28)$$

Using the adiabatic shock conditions *i.e.*, (24-26), the supersonic branch temperature and bulk velocity can be obtained from post-shock quantities and vice versa,

$$\vartheta_-^2 - 2(c_1 - h_-) = 0 \quad \text{and} \quad \Theta_- = \frac{K}{2}(c_0\vartheta_- - \vartheta_-^2), \quad (29)$$

here,  $c_0 = (1 - R_{\dot{m}})[2\Theta_+/K + \vartheta_+^2]/\vartheta_+$  and  $c_1 = \vartheta_+^2/2 + h_+$ . Both the expressions  $(\vartheta_-, \Theta_-)$  in eq. 29 are obtained simultaneously in terms of post-shock quantities which gives us the shock location  $x_s$ .

In case of dissipative shocks, we use eqs.(24, 25, 27) to relates post-shock and pre-shock quantities. The relation is,

$$\vartheta_- = \sqrt{2(c_d - h_-(1 + f_e))}, \text{ and, } \Theta_- = \frac{K}{2}(c_0\vartheta_- - \vartheta_-^2), \quad (30)$$

where,  $c_d = \vartheta_+^2/2 + h_+(1 + f_e)$ .

For isentropic shocks, we use eqs. (24, 25, 28) to obtain,

$$\vartheta_- \exp(k_{3-}) \Theta_-^2 (3\Theta_- + 2)^{k_1} (3\Theta_- + 2/\eta)^{k_2} - c_{e0} = 0; \text{ and, } \Theta_- = \frac{K}{2} (c_0 \vartheta_- - \vartheta_-^2), \quad (31)$$

where,  $c_{e0} = \vartheta_+ \exp(k_{3+}) \Theta_+^2 (3\Theta_+ + 2)^{k_1} (3\Theta_+ + 2/\eta)^{k_2}$ . We will briefly show the three shock transitions in the  $\mathcal{E} - \dot{\mathcal{M}}$  parameter space, and the related solutions (see Fig. 4). However, in the rest of the paper, we will concentrate on adiabatic shocks and the resulting mass outflow rate.

#### 2.2.4 Outflow

Simulations (Molteni *et al.* 1996; Giri & Chakrabarti 2013) have shown that extra thermal gradient force along the vertical direction, drives bipolar outflows, therefore the outflow and the accretion solution is connected by the shock. As has been suggested by Molteni *et al.* (1996) and is described in details by Kumar & Chattopadhyay (2013), the outflowing matter tend to move out through the region between the funnel wall (FW) and the centrifugal barrier (CB). The cylindrical radius of the CB is,

$$x_{CB} = [2\lambda^2 r_{CB} (r_{CB} - 1)^2]^{\frac{1}{4}}, \quad (32)$$

and that of FW is,

$$x_{FW}^2 = \lambda^2 \frac{(\lambda^2 - 2) + \sqrt{(\lambda^2 - 2) - 4(1 - y_{CB}^2)}}{2}, \quad (33)$$

where, the spherical radius of CB is  $r_{CB} = (x_{CB}^2 + y_{CB}^2)^{1/2}$ , while  $y_{CB}$  is the local height of CB. The streamline is computed as,  $r_j = \sqrt{x_j^2 + y_j^2}$ , where  $x_j = (x_{FW} + x_{CB})/2$ , and  $y_j = y_{FW} = y_{CB}$ . The cross-sectional area of the jet is defined as,

$$\mathcal{A} = \frac{2\pi(x_{CB}^2 - x_{FW}^2)}{\sqrt{1 + (dx_j/dy_j)^2}}. \quad (34)$$

The momentum balance equation along the jet stream line is given by

$$\vartheta_j \frac{d\vartheta_j}{dr} + \frac{1}{\rho_j} \frac{dp_j}{dr} - \frac{\lambda_j^2}{x_j^3} \frac{dx_j}{dr} + \frac{1}{2(r_j - 1)^2} \frac{dr_j}{dr} = 0, \quad (35)$$

here the derivative is with respect to  $r = r_{CB}$ . Suffix ‘j’ denotes jet quantities. The integrated continuity equation along the jet stream line is given by

$$\dot{M}_{out} = \rho_j \vartheta_j \mathcal{A} \quad (36)$$

This integration constant is called as mass flux which is moving along the stream line of jet. By using eqs. (16, 36), we can write entropy-outflow rate of the jet.

$$\dot{M}_{out} = \frac{\dot{M}_{out}}{2\pi\mathcal{K}} = \exp(k_3)\Theta_j^{3/2}(3\Theta_j + 2)^{k_1}(3\Theta_j + 2/\eta)^{k_2}\vartheta_j\frac{\mathcal{A}}{2\pi}. \quad (37)$$

Now, using eqs.(6,36) in eq.(15), we get

$$\frac{d\Theta_j}{dr} = -\frac{\Theta_j}{N} \left[ \frac{1}{\vartheta_j} \frac{d\vartheta_j}{dr} + \frac{1}{\mathcal{A}} \frac{d\mathcal{A}}{dr} \right] \quad (38)$$

The jet velocity gradient equation obtain by combining eqs.(8, 35-38), we get

$$\frac{d\vartheta_j}{dr} = \frac{N_j}{D_j}. \quad (39)$$

where,

$$N_j = \frac{a_j^2}{\mathcal{A}} \frac{d\mathcal{A}}{dr} + \frac{\lambda_j^2}{x_j^3} \frac{dx_j}{dr} - \frac{1}{2(r_j - 1)^2} \frac{dr_j}{dr}$$

and

$$D_j = \vartheta_j - \frac{a_j^2}{\vartheta_j}.$$

The critical point conditions are,

$$a_{jc}^2 = \left[ \frac{1}{\mathcal{A}_c} \frac{d\mathcal{A}_c}{dr} \right]^{-1} \left[ \frac{1}{2(r_{jc} - 1)^2} \frac{dr_j}{dr} - \frac{\lambda_j^2}{x_{jc}^3} \frac{dx_j}{dr} \right] \quad \& \quad \vartheta_{jc} = a_{jc}. \quad (40)$$

The derivatives at  $r_{jc}$  is obtained as,

$$\left( \frac{d\vartheta_j}{dr} \right)_{r_c} = \left( \frac{dN_j/dr}{dD_j/dr} \right)_{r_c}; \quad \left( \frac{d\Theta_j}{dr} \right)_{r_c} = -\frac{\Theta_{jc}}{N_c} \left[ \frac{1}{\vartheta_{jc}} \left( \frac{d\vartheta_j}{dr} \right)_{r_c} + \frac{1}{\mathcal{A}_c} \left( \frac{d\mathcal{A}}{dr} \right)_{r_c} \right] \quad (41)$$

The subscript  $c$  denotes the quantities at critical point in the outflow.

So, the mass outflow rate in term of flow variables at the shock front is given by,

$$R_{in} = \frac{\dot{M}_{out}}{M_{in}} = \frac{1}{[2\pi\Sigma_+\vartheta_+r_s/(\rho_j\vartheta_j(r_{cb})\mathcal{A}(r_{cb})) + 1]} \quad (42)$$

where,  $\rho_j = \rho(r_b)\exp(-x_j/h(r_b))$ ,  $\vartheta_j(r_{cb})$  and  $\mathcal{A}(r_{cb})$  are jet base density, base velocity and base cross section, respectively. Here,  $r_b = (x_{ci} + x_s)/3$  and  $r_{CB} = r = \sqrt{r_b^2 + h_b^2}$ ,  $h_b$  being the height of the disc at  $r_b$ . The angular momentum of the jet  $\lambda_j = \lambda|_{(x=r_b)} = \lambda$ , *i.e.*, the jets are launched with the angular momentum of the accretion disc at the base of the jet, and since presently we assume inviscid flow, the jet and the accretion disc has the same angular momentum.

### 2.2.5 Solution Procedure

The solution procedure is the following, given  $\mathcal{E}$ ,  $\lambda$ ,  $\xi$  the sonic points of the accretion discs are computed. If there is only one sonic point, one integrates eqs. (18,19) inwards and outwards starting from the sonic point and using the sonic point conditions (eqs. 20-23). In the multiple critical (or sonic) point regime *i.e.*,MCP regime, we may start with either  $x_{ci}$

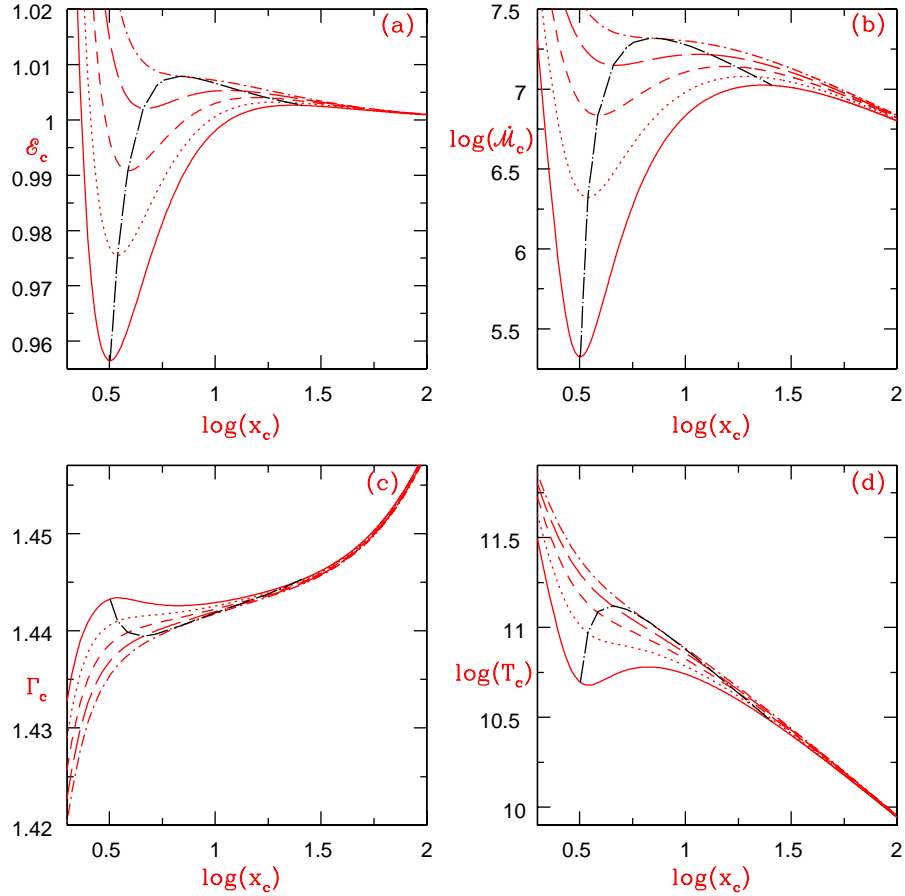


**Figure 1.** (a)  $\mathcal{E}_c$ , the specific energy at  $x_c$ , (b) entropy accretion rate ( $\dot{\mathcal{M}}_c$ ) at  $x_c$ , (c)  $\Gamma_c$  and (d)  $\log(T_c)$  is plotted with  $\log(x_c)$  for  $\xi = 1$  and for  $\lambda = 1.75$  (solid), 1.65 (dotted), 1.55 (dashed), 1.45 (long-dashed), and 1.35825 (dashed-dotted). Long dashed-dotted curve is the loci of maxima and minima of the curves and represents the part of the parameter space which gives multiple critical points(MCP).

or  $x_{co}$  and solve eqs. (18-23) to obtain the solutions. In case the flow parameters  $\mathcal{E}$ ,  $\lambda$ ,  $\xi$  fall in the MCP domain, we also check for the shock conditions (eqs. 24-26) as we integrate the equations of motion. In the first iteration we assume  $R_{\dot{m}} = 0$ . If the shock conditions are satisfied, then the solution will jump from the supersonic branch to the subsonic branch. In this paper, we have always started our integration from  $x_{ci}$  if the parameters belonged to the MCP domain, and therefore by locating shock through eqs. (24-26) or equivalently eq. (29), the solution will jump to the supersonic branch through  $x_{co}$ . Once the shock is found, we solve eqs. (39-38) to find the jet solutions and the corresponding  $R_{\dot{m}}$  (eq. 42). This value of  $R_{\dot{m}}$  is supplied to eq. (29) and the whole solution procedure is repeated to obtain another shock location. This is repeated till the shock location converges.

### 3 RESULTS

#### 3.1 Nature of critical points and accretion flow solutions

We discuss the properties of the sonic points of the flow around blackholes with an approximate relativistic equation of state and how they are affected by  $\xi$  and  $\lambda$  parameters. We plot  $\mathcal{E}_c$  (Fig. 1a),  $\dot{\mathcal{M}}_c$  (Fig. 1b),  $\Gamma_c$  (Fig. 1c) and  $\log(T_c)$  (Fig. 1d) with  $\log(x_c)$  for  $\xi = 1$  or electron-proton flow (hereafter  $e^- - p^+$ ), and for  $\lambda = 1.75$  (solid), 1.65 (dotted), 1.55 (dashed), 1.45 (long-dashed), and 1.35825 (dashed-dotted). For low  $\lambda$  ( $< 1.35825$ ) there is only one sonic point for any value of  $\mathcal{E}$ , however, the number of sonic points increase with increasing  $\lambda$ . Moreover,  $\Gamma_c$  depend on the location of the sonic point. Lower temperature at the sonic point or  $T_c$  implies lower  $\mathcal{E}_c$ ,  $\dot{\mathcal{M}}_c$  and higher  $\Gamma_c$ . Since  $\Gamma \rightarrow 5/3$  means non-relativistic thermal energy and  $\Gamma \rightarrow 4/3$  implies ultra-relativistic thermal energy, so higher temperature implies lower  $\Gamma$ . The extrema of  $\mathcal{E}_c(x_c)$  and  $\dot{\mathcal{M}}_c(x_c)$  are joined by the long dashed-dotted curve in the figures which shows the domain of the parameters which supports multiple critical points (MCP).

To see how the sonic point or the critical point properties are affected by  $\xi$ , we plot  $\mathcal{E}_c$  (Fig. 2a),  $\dot{\mathcal{M}}_c$  (Fig. 2b),  $\Gamma_c$  (Fig. 2c) and  $\log(T_c)$  (Fig. 2d) with  $\log(x_c)$ , for  $\lambda = 1.65$ , and  $\xi = 1.0$  (solid), 0.75 (dotted), 0.5 (dashed), 0.25 (long-dashed), 0.1 (dashed-dotted) and 0.0 (long dashed-dotted). For flows with  $1.0 \geq \xi > 0.0$  a maxima and a minima in  $\mathcal{E}_c$  and  $\dot{\mathcal{M}}_c$  exist, however for  $\xi = 0.0$  there is only a minima and no maxima. Closer inspection reveals that for  $\xi = 0$  or pair plasma flow or  $e^- - e^+$  flow, the physical X type sonic points are formed closer to the horizon, which means, no matter what the value of  $\lambda$ , only one sonic point will form for  $e^- - e^+$  flow, or for any flow described by single species EoS. As we have mentioned in §2.2.2, that sonic points can only be harboured by hot flows, and Fig. 2d shows that  $T_c$  is the lowest for  $e^- - e^+$  flow (long dashed-dotted). A flow is thermally relativistic if its thermal energy is comparable to its rest energy *i.e.*,  $\Theta = kT/m_e c^2 \gtrsim 1$ , and the adiabatic index will be reflected by a value  $4/3 \leq \Gamma < 5/3$ . Although,  $e^- - e^+$  is the lightest flow, its  $T_c$  is so low that for most values of  $x_c$ ,  $\Gamma_c \sim 5/3$  (long dashed-dotted in Fig. 2c). Therefore, at a large distance away from the black hole, physical sonic points are not formed. Closer to the horizon, the flow is hot enough to produce one physical sonic point. As  $\xi$  increases, the rest energy increases but the temperature increases even more, which makes flow with protons much hotter and thermally more relativistic (Fig. 2c). Therefore, for a given  $\mathcal{E} > 1$ , one or more sonic points may form.

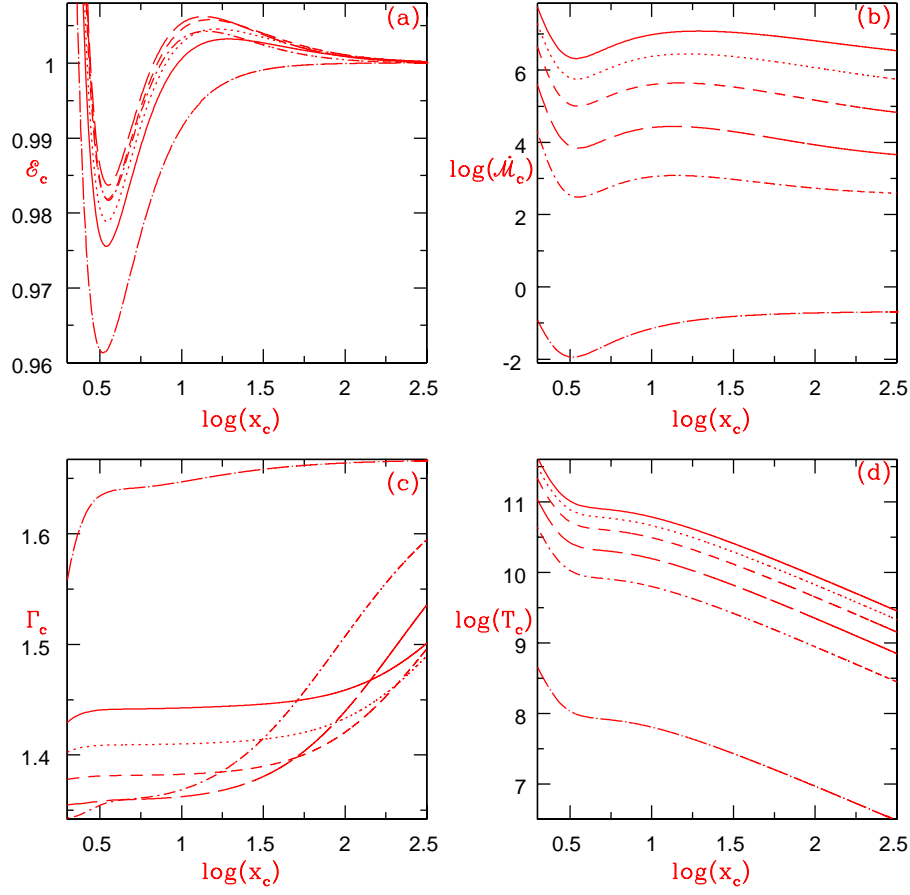


**Figure 2.** (a)  $\mathcal{E}_c$ , the specific energy at  $x_c$ , (b) entropy accretion rate ( $\dot{M}_c$ ) at  $x_c$ , (c)  $\Gamma_c$  and (d)  $\log(T_c)$  is plotted with  $\log(x_c)$  for  $\lambda = 1.65$  and for  $\xi = 1.0$  (solid),  $0.75$  (dotted),  $0.5$  (dashed),  $0.25$  (long-dashed),  $0.1$  (dashed-dotted) and  $0.0$  (long dashed-dotted).

One may join the maxima and minima of the  $\mathcal{E}_c(x_c)$  and the corresponding  $\lambda$ -s for a given  $\xi$ , and plot in  $\mathcal{E} - \lambda$  plane, the resulting bounded region gives the values of  $\mathcal{E}$ ,  $\lambda$  which supports multiple sonic points, and are abbreviated as MCP region (multiple critical point). In Fig. 3a, we plot the MCP for  $\xi = 1.0$  or  $e^- - p^+$  (solid),  $\xi = 0.75$  (dotted),  $\xi = 0.5$  (dashed) and  $\xi = 0.27$  (long-dashed), while in Fig. 3b, we plot  $\xi = 0.2$  (solid),  $\xi = 0.1$  (dotted),  $\xi = 0.05$  (dashed) and  $\xi = 0.01$  (long-dashed). It shows that as  $\xi$  is reduced, the reduction of rest energy is making the flow more energetic and relativistic, so the MCP shifts to higher energy, higher angular momentum side. This continues till  $\xi = 0.27$ . Any further reduction of  $\xi$ , reduces the temperature to the extent that simultaneous reduction in rest energy cannot compensate for the lack of thermal energy, and the flow becomes less energetic and less relativistic, compared to flow of  $\xi = 0.27$ . The MCP shifts to the less energetic and lower angular momentum part of the parameter space, with simultaneous reduction in the area of the MCP which finally vanishes for  $\xi = 0.0$ .

The sonic point properties not only tell us about the number of sonic points, but also

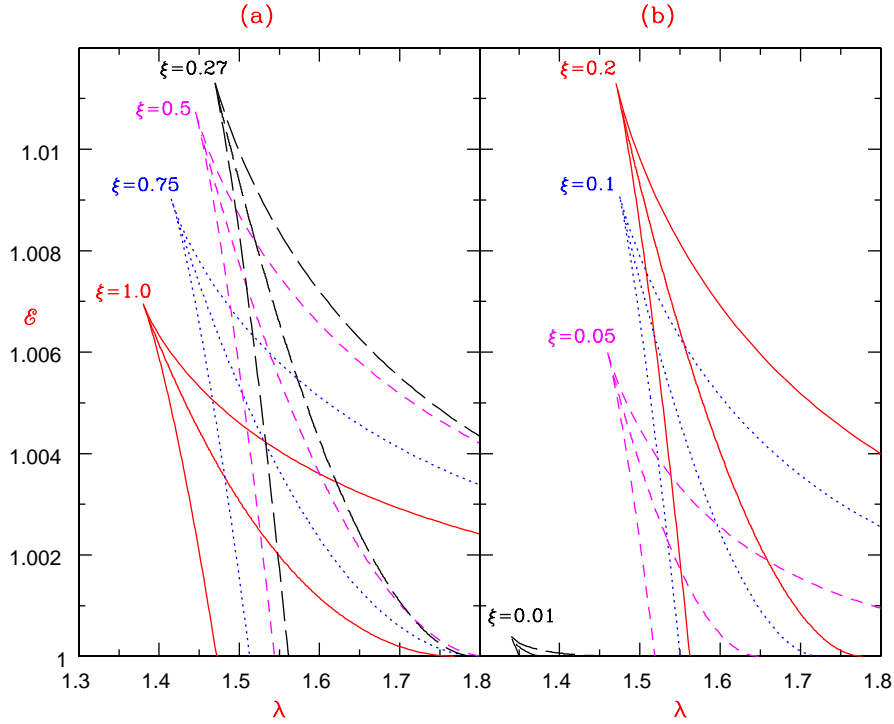


**Figure 3.**  $\mathcal{E} - \lambda$  parameter space represents multiple critical points (MCP) domain for (a)  $\xi = 1.0$  (solid),  $\xi = 0.75$  (dotted),  $\xi = 0.5$  (dashed) and  $\xi = 0.27$  (long-dashed) and (b)  $\xi = 0.2$  (solid),  $\xi = 0.1$  (dotted),  $\xi = 0.05$  (dashed) and  $\xi = 0.01$  (long-dashed).

tells us about the very nature of transitions in the solution. In Fig. 4, we plot  $\mathcal{E}_c$  with  $\dot{\mathcal{M}}_c$  for  $\lambda = 1.6$  and  $\xi = 1.0$ . The inner sonic point quantities are plotted along  $MN$ , while middle and outer sonic point quantities are  $NO$  and  $OQ$ , respectively. Adiabatic shocks occur parallel to the  $\dot{\mathcal{M}}_c$  axis, *i.e.*, along  $S_4 \rightarrow S_1$ , the  $T_1$  inset shows the actual Mach number ( $M = v/a$ ) solution of such a transition (Eq. 29). Equation 30 represents the dissipative shock shown by  $S_4 \rightarrow S_2$  or  $T_2$  transition. An isentropic shock is parallel to the ordinate represented by eq. 31, and by the transition  $S_4 \rightarrow S_3$  or  $T_3$  transition. The energy and entropy jumps for the respective transitions are marked in the Figure. We plot  $\mathcal{E}_c$  with  $\dot{\mathcal{M}}_c$  for  $\lambda = 1.6$  and  $\xi = 1.0$  (Fig. 5a),  $\xi = 0.1$  (Fig. 5b),  $\xi = 0.035$  (Fig. 5c) and  $\xi = 0.0$  (Fig. 5d). For a flow with a significant proton proportion, all the branches for multispecies flow are obtained. However, as the proton proportion is decreased, the outer critical point branch starts to get shortened, and actually disappears for  $\xi = 0.0$ . This implies there cannot be any steady state shock transitions for  $\xi = 0.0$ .

Various flow quantities of only the accretion disc (*i.e.*, without allowing for mass loss) are

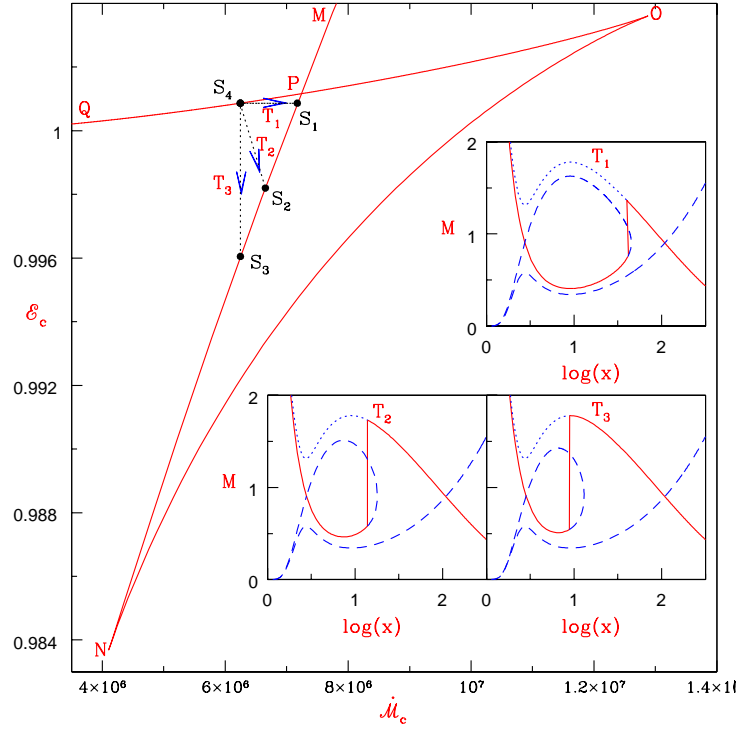


**Figure 4.** Plot of  $\mathcal{E}_c$  with  $\dot{\mathcal{M}}_c$  for  $\lambda = 1.6$  and  $\xi = 1.0$ . Branches  $MN, NO$  and  $OQ$  corresponds to inner, middle and outer critical points of the flow, respectively. The adiabatic shock transition  $T_1$  shown as  $S_4 \rightarrow S_1$ , the dissipative shock  $T_2$ , shown as  $S_4 \rightarrow S_2$  and isentropic shock  $T_3$ , shown as  $S_4 \rightarrow S_3$ . The solutions corresponding to transitions  $T_1, T_2, T_3$  are shown in the inset, where solid curves represent accretion flows with shocks. The coordinates of the transitions are  $S_1(\mathcal{E} = 1.0087, \dot{\mathcal{M}} = 7.17 \times 10^6)$ ,  $S_2(\mathcal{E} = 0.9982, \dot{\mathcal{M}} = 6.65 \times 10^6)$ ,  $S_3(\mathcal{E} = 0.99605, \dot{\mathcal{M}} = 6.25 \times 10^6)$ , and  $S_4(\mathcal{E} = 1.0087, \dot{\mathcal{M}} = 6.25 \times 10^6)$ .

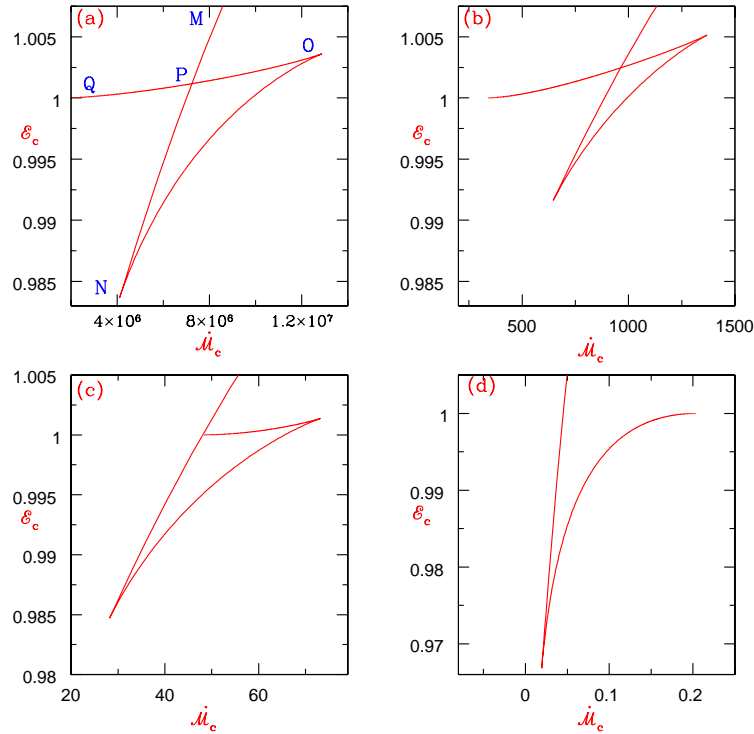


**Figure 5.**  $\mathcal{E}_c$  is plotted with  $\dot{\mathcal{M}}_c$  for  $\lambda = 1.6$  for various (a)  $\xi = 1.0$ , (b)  $\xi = 0.1$ , (c)  $\xi = 0.035$ , and (d)  $\xi = 0.0$ .



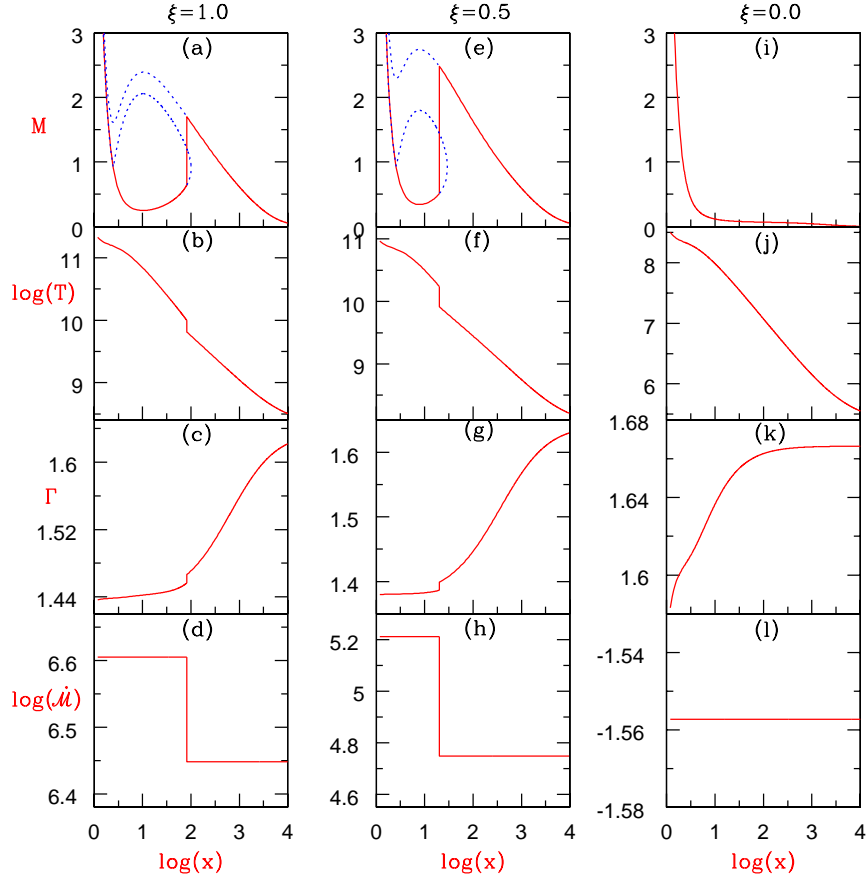


**Figure 6.** Various accretion flow quantities are plotted with radial distance [ $\log(x)$ ]: (a, e, i) Mach number ( $M$ ), (b, f, j) temperature ( $T$ ), (c, g, k) adiabatic index ( $\Gamma$ ) and (e, h, l) entropy accretion rate ( $\dot{M}$ ) for the accretion disc parameters,  $(\mathcal{E}, \lambda) = (1.0001, 1.68)$  with  $\xi = 1.0$  (a-d), 0.5 (e-h) and 0.0 (i-l).

plotted in Figs. 6a-l. The flow variables are  $M$  (Figs. 6a, e, i),  $T$  (Figs. 6b, f, j),  $\Gamma$  (Figs. 6c, g, k) and  $\dot{M}$  (Figs. e, h, l) as a function of the radial distance [ $\log(x)$ ]. From Figs. 3a-b, it can be shown that for a particular  $\mathcal{E}$  &  $\lambda$ , if one  $\xi$  value produces multiple critical points, then another  $\xi$  can exhibit only one sonic point. However, for Figs. 6a-l, we have chosen a value of  $\mathcal{E}$  &  $\lambda$  which admits shock solutions for a wide range of  $\xi$  ( $= 1 \rightarrow 0.087$ ). In Figs. 6a-l, we consider the same  $(\mathcal{E}, \lambda) = (1.0001, 1.68)$ , but different compositions:  $e^- - p^+$  or  $\xi = 1.0$  (in Figs. 6a-d),  $\xi = 0.5$  (in Figs. 6e-h), and  $e^- - e^+$  or  $\xi = 0.0$  (in Figs. 6i-l). The temperature and the entropy is higher for higher  $\xi$ , and the shock location is also at a larger distance for flow with higher  $\xi$ . Figures 6c, g & k, show  $\Gamma$  is variable for flows with any  $\xi$ . At  $x \rightarrow$  large,  $\Gamma \sim 5/3$ , irrespective of the value of  $\xi$ . However, since  $\xi = 0.0$  flow has very low thermal energy,  $\Gamma \sim 5/3$  up to  $x \sim 100$ . But for flows with  $\xi \neq 0.0$ , we find  $\Gamma_{\xi=0.5} < \Gamma_{\xi=1.0}$  at  $x < \text{few} \times 100$ . At  $x \sim 1$ ,  $\Gamma_{\xi=0.5} \sim 1.4$ ,  $\Gamma_{\xi=1.0} \sim 1.44$ . This means that the flow becomes thermally more relativistic with the reduction of  $\xi$  up to a certain value (*i.e.*, around  $\xi \sim 0.27$ ), and then becomes less relativistic with further reduction of  $\xi$ .

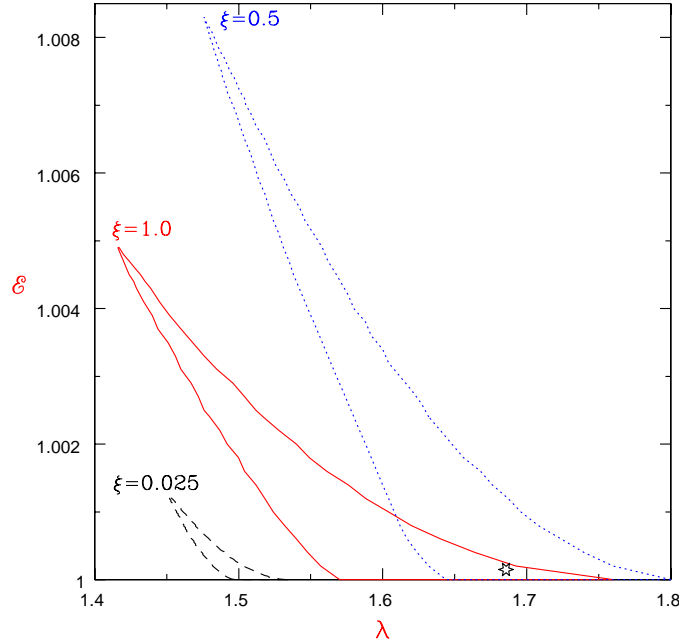


**Figure 7.** Parameter spaces producing shocks without any mass loss: for  $\xi = 1.0$  or  $e^- - p^+$  (solid),  $\xi = 0.5$  (dotted) and  $\xi = 0.025$  (dashed).  $e^- - e^+$  or  $\xi = 0.0$  flow does not admit standing accretion shock solution. The star marks the parameters with which solutions in Figs. 6a-l, were generated.

Although  $\xi = 0.5$  and  $e^- - p^+$  flow for the chosen value of  $\mathcal{E}$  &  $\lambda$  harbours shocks, but shock location and other flow parameters are quite different.  $e^- - e^+$  being the coldest, slowest and showing only a single sonic point, is significantly different from any flow with  $\xi \neq 0.0$ .

In Fig. 7, we plot the sub-domain of MCP in the  $\mathcal{E} - \lambda$  parameter space which admits standing shock solutions, for three  $\xi$  values, and they are  $\xi = 1.0$  (solid),  $\xi = 0.5$  (dotted), and  $\xi = 0.025$  (dashed). Similar to Figs. 3a-b, the shock parameter space also shows a shift to the more energetic part of the parameter space with the decrease of  $\xi$ . As it has been explained, that the reduction of  $\xi$  reduces the rest energy of the flow, making the flow more relativistic as well as more energetic. But reduction of  $\xi$  entails a reduction of  $T$  as well, and for proton poor flows (*i.e.*,  $\xi \rightarrow 0$ ) the temperature is so low that it becomes thermally non-relativistic as well as less energetic. Hence if the shock can at all be supported, it occurs in a low energy and low angular momentum part of the parameter space. For  $\xi = 0$  shock in accretion is totally absent and therefore the shock parameter space for  $e^- - e^+$  flow does not appear in the  $\mathcal{E} - \lambda$  space. The star mark indicates the values of  $\mathcal{E}$  &  $\lambda$  which were used to obtain the solutions of Figs. 6a-l.

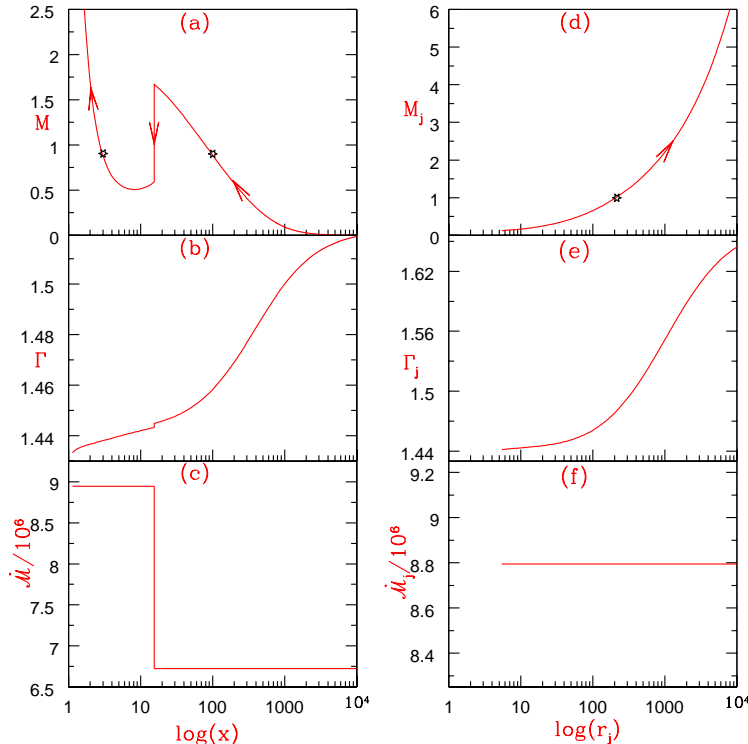


**Figure 8.** Accretion-jet solution for  $e^- - p^+$  flow, for  $\mathcal{E} = 1.001$ ,  $\lambda = 1.56$ . The accretion shock denoted by the vertical jump is at  $x_s = 15.306$ . The accretion flow variables  $M$  (a),  $\Gamma$  (b) and the entropy-accretion rate  $\dot{\mathcal{M}}$  (c) are plotted with  $x$ . The jet variables  $M_j = \vartheta_j/a_j$  (d),  $\Gamma_j$  (e), and  $\dot{\mathcal{M}}_j$  (f) plotted with jet radial coordinate  $r_j$ . Arrows show the direction of the flow and the stars denote the critical or sonic points of the flow.

### 3.2 Accretion and ejection solutions

In this Section, we present self-consistent accretion-ejection solutions. The methodology to simultaneously and self-consistently compute the accretion-ejection solution has been presented in Section 2.2.5. In Figs. 8a-c, the accretion disc flow quantities like  $M$  (a),  $\Gamma$  (b), and  $\dot{\mathcal{M}}$  (c) are plotted as a function of radial distance. In Figs. 8d-f, the jet flow quantities *e.g.*,  $M_j$  (d),  $\Gamma_j$  (e), and  $\dot{\mathcal{M}}_j$  (f) are plotted as a function of  $r_j$ . The constituent of the flow of the disc-jet system presented in this Figure is  $\xi = 1.0$ . Other flow parameters are:  $\mathcal{E} = 1.001$ ,  $\lambda = 1.56$ . The accretion disc solution admits an accretion shock at  $x_s = 15.306$  (vertical jump in Figs. 8a-c), and launches a thermally driven bipolar jet whose sonic point is at  $r_{jc} = 209.139$ . The relative mass outflow rate is  $R_{\dot{m}} = 0.038$ . The jet starts with the  $\Gamma$  value of the post-shock disc but since it is thermally driven and is powered by converting the thermal energy to kinetic energy,  $\Gamma$  approaches non-relativistic values far away from the central object. At the shock, the entropy of the jet jumps up from pre-shock to post-shock value (Fig. 8c). Interestingly, the entropy of the jet is also much higher than the pre-shock disc. This entropy condition ensures that although most of the matter flows through the inner sonic point into the black hole, a significant amount of matter also flows out as jet.

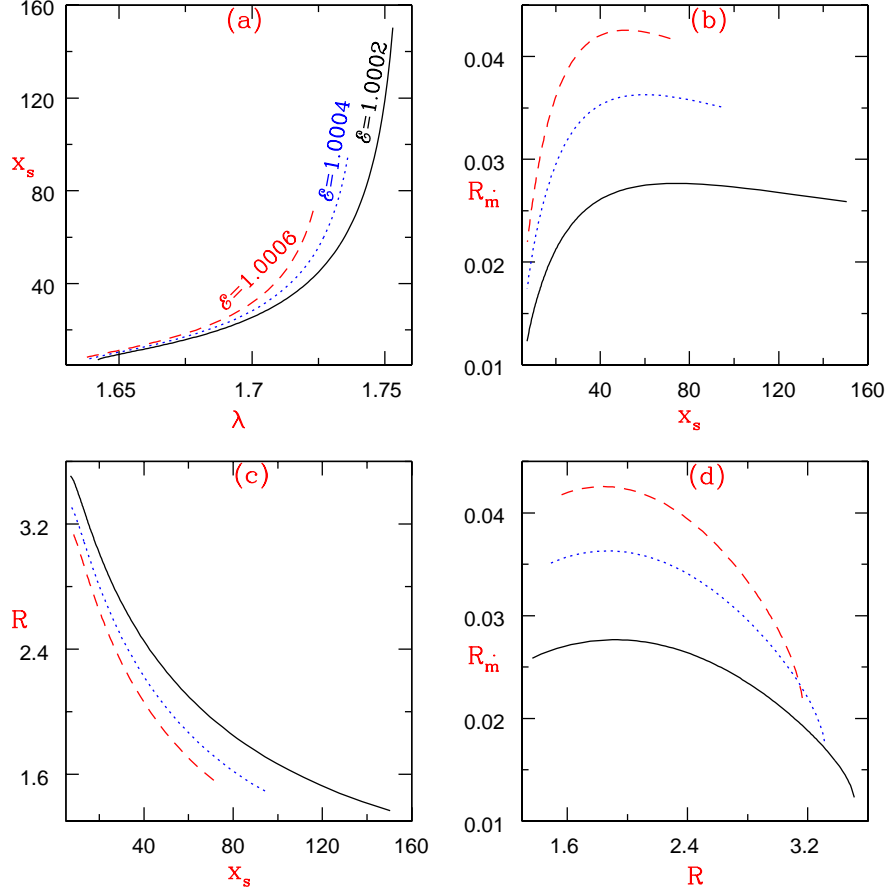


**Figure 9.** Plot of (a)  $x_s$  with  $\lambda$ , (b)  $R_m$  with  $x_s$ , (c) Compression ratio  $R$  with  $x_s$  and (d)  $R_m$  with  $R$ . Each curve corresponds to  $\mathcal{E} = 1.0002$  (solid), 1.0004 (dotted), and 1.0006 (dashed).

Now we plot  $x_s$  with  $\lambda$  (Fig. 9a),  $R_m$  with  $x_s$  (Fig. 9b), compression ratio  $R = \Sigma_+/\Sigma_-$  with  $x_s$  (Fig. 9c), and  $R_m$  with  $R$  (Fig. 9d), the composition of the flow is given by  $\xi = 0.27$ . Parameters for each curve is  $\mathcal{E} = 1.0002$  (solid), 1.0004 (dotted), and 1.0006 (dashed). For a given value of  $\lambda$ ,  $x_s$  increases with  $\mathcal{E}$ . Similarly for a given  $x_s$ ,  $R_m$  increases with  $\mathcal{E}$ , but  $R$  decreases with the increasing  $\mathcal{E}$ . This obviously means  $R_m$  increases with  $\mathcal{E}$ . Interestingly, the dependence of  $R_m$  with  $R$  for a given  $\mathcal{E}$ , qualitatively follows the pattern of Chakrabarti (1999). For a given  $\mathcal{E}$ ,  $x_s$  decreases with decreasing  $\lambda$ . This increases the compression, and drives more matter into the jet channel. But with decreasing  $x_s$ , the post-shock area decreases too, and that also limits the total amount of matter leaving the disc. Hence  $R_m$  will depend on increasing  $R$ , as well as the decreasing total post-shock area, and hence  $R_m$  peaks at some intermediate value of  $R$ .

Keeping  $\mathcal{E} = 1.0003$ , we now vary  $\lambda$ , of flow with following compositions  $\xi = 1.0$  (solid),  $\xi = 0.635$  (dotted), and  $\xi = 0.27$  (dashed). We plot  $x_s$  with  $\lambda$  (Fig. 10a),  $R_m$  with  $x_s$  (Fig. 10b),  $R$  with  $x_s$  (Fig.10c), and  $R_m$  with  $R$  (Fig. 10d). We reconfirm that indeed  $R_m$  increases

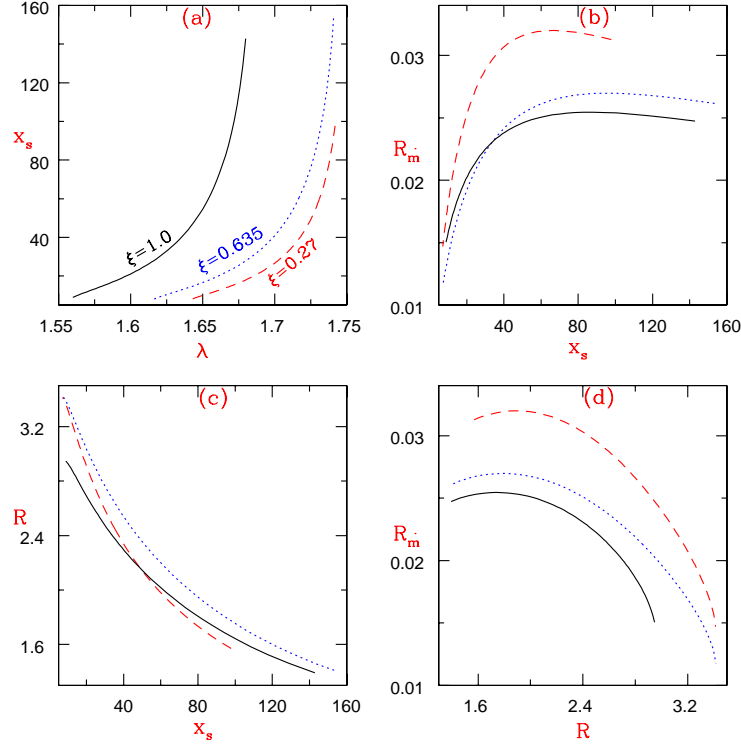


**Figure 10.** (a) Plot of  $x_s$  with  $\lambda$ , (b)  $R_{\dot{m}}$  with  $x_s$ , (c)  $R$  with  $x_s$ , and (d)  $R_{\dot{m}}$  with  $R$  for  $\mathcal{E} = 1.0003$ . Each curve corresponds to  $\xi = 1.0$  (solid),  $0.635$  (dotted), and  $0.27$  (dashed).

with the increasing  $R$  or decreasing  $x_s$ , although decreasing post-shock surface area finally decreases  $R_{\dot{m}}$ .  $R_{\dot{m}}$  is highest for  $\xi = 0.27$ , compared to flow of other compositions. To ensure this we scan the entire  $\mathcal{E}$  &  $\lambda$  parameter space for a given value of  $\xi$ , and find out the maximum mass outflow rate possible for that particular  $\xi$ . In Fig. 11, we plot the maximum mass-outflow rate *i.e.*,  $R_{\dot{m}}^m = \max(R_{\dot{m}})$ , as a function of  $\xi$ . It easily shows that maximum outflow is possible for  $\xi = 0.27$ .

In Figs. 12a-b, we show the parameter space where standing shocks form (the so-called ‘shock-domain’) for various  $\xi$ . Similar to the behaviour of MCP domain, the shock domain in  $\mathcal{E} - \lambda$  parameter space shifts to the higher energy and angular momentum region as  $\xi$  is decreased from its  $e^- - p^+$  value up to  $\xi = 0.27$ . If  $\xi$  is decreased further, the flow becomes less energetic and the shock-domain moves towards the lower energy and lower angular momentum corner, with subsequent decrease in the bounded area of the shock space. Finally, the shock domain disappears for  $\xi = 0.0$ . In Fig. 12c, we compare the shock domain for  $\xi = 1.0$ , of the accretion flow which includes mass loss (solid) and which does not include mass loss (dotted). In Fig. 12d, we compare the shock domain for  $\xi = 0.25$ , of the accretion flow which includes mass loss (solid) and which does not mass loss (dotted). This shows that the reduction of post-shock pressure due to mass loss, reduces the steady shock

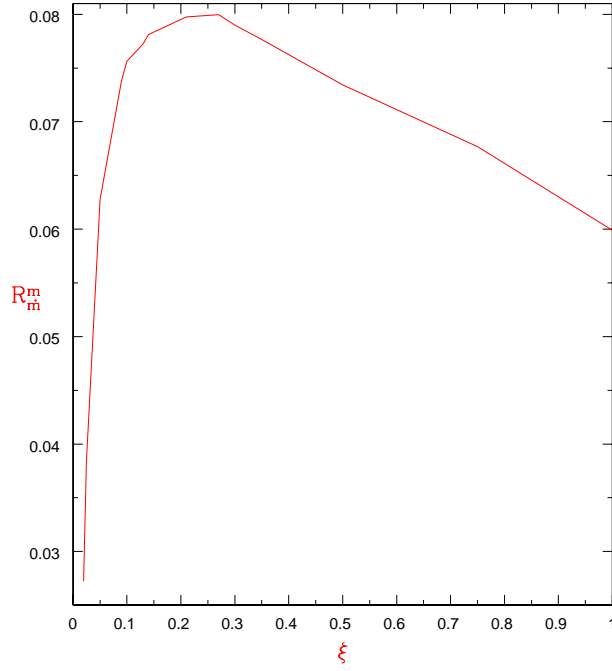


**Figure 11.** The plot of maximum mass outflow rate  $R_m^m$  with the composition parameter  $\xi$ .

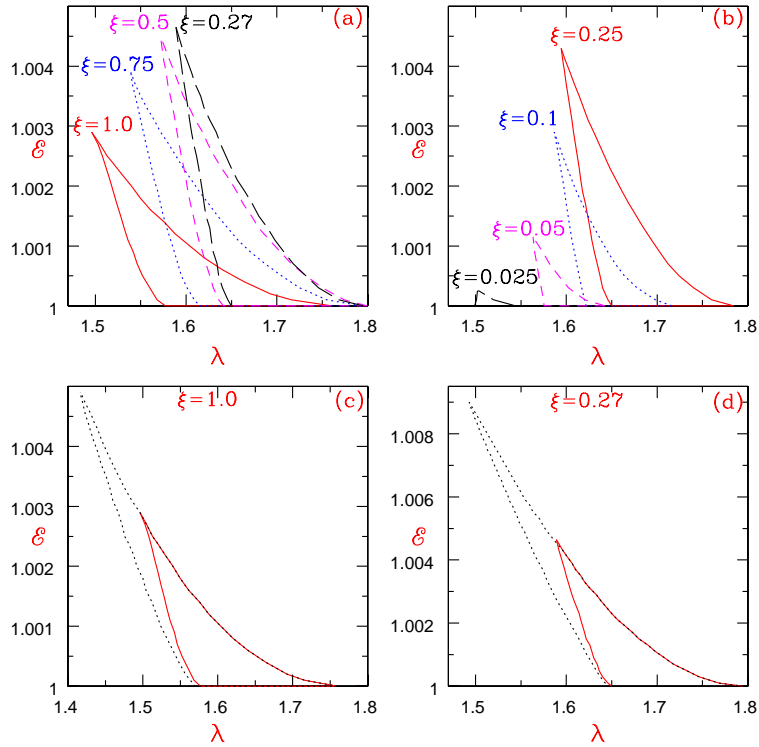


**Figure 12.** Shock-domain in the  $\mathcal{E} - \lambda$  parameter space with mass loss. Flow composition  $\xi$  is marked. (a) Parameter space for  $\xi = 1.0 \rightarrow 0.27$  and (b) for  $\xi = 0.25 \rightarrow 0.025$ . (c) Comparison of the domains in  $\mathcal{E} - \lambda$  space with mass loss (solid) and without mass loss (dotted) for  $\xi = 1.0$  and (d) Comparison of the 'shock-domain' with mass loss (solid) and without mass loss (dotted) for  $\xi = 0.27$ .

domain. Flow from that part of the parameter space which admits shock without massloss, actually do not show steady shock when massloss is allowed. So there is a possibility of massloss driven shock oscillation too.

#### 4 DISCUSSION AND CONCLUDING REMARKS

In this paper, we studied the outflow behaviour taking into account flow composition and approximate relativistic equation of state of the flow onto black holes. We have re-established our earlier findings that  $e^- - e^+$  is the least relativistic flow, but  $e^- - p^+$  is not the most relativistic flow. Thermally, the most relativistic flow is when  $\xi = 0.27$ . As has been explained earlier, the flow starting with the same  $\mathcal{E}$  implies a flow starting with the same sound speed at infinity. Since the sound speed is a measure of the thermal speed, if we compare two flows with the same thermal speed, the constituent particles will transfer less average kinetic energy (*i.e.*, thermal energy) in the flow where these particles are lighter. Therefore, the temperature of  $e^- - e^+$  flow is lesser than the flow containing both electrons (and/or positrons) and heavier protons. The temperature of  $e^- - e^+$  is so low that the lower inertia of the flow cannot compensate for its lack of thermal energy and therefore thermally it is the least relativistic, while the flow with some amount of protons are more relativistic. Although the conclusions are consistent with the previous papers (Chattopadhyay 2008; Chattopadhyay & Ryu 2009; Chattopadhyay & Chakrabarti 2011), in this paper, we derived the analytical form of the adiabatic equation of state for multispecies flow (*e.g.*, eq. 16). Using the adiabatic equation of state, we present the form of the entropy-mass flow rate for accretion (eq. 17), as well as for outflow (eq. 37). Since the  $e^- - e^+$  flow is not hot enough, they show only one physical sonic point, and has been shown in this paper. However, the flow with some amount of protons show formation of multiple sonic points and shocks.

Post-shock disc drives bipolar outflows. The mass outflow rate is calculated self-consistently and is found to be around a few percent. Interestingly, the mass outflow rate is also generally higher for flows with  $\xi \sim 0.27$ . Since, the shock forms at a larger distance for flows with a higher angular momentum, the mass outflow rate is also generally lower for high angular momentum flow. The mass outflow rate depends on many factors, the shocks location, the angular momentum, energy or composition of the accretion flow. If the shock location is smaller (say for lower angular momentum), the compression ratio is larger, and the mass outflow increases. But we have shown that the mass outflow rate do not increase monoton-

ically with the compression ratio, rather the mass outflow rate peaks at some intermediate value. We also plotted the parameter space for the shock in presence of the mass loss. Due to the loss of matter, the post-shock pressure is reduced, and therefore the entire range of parameters for which steady shock condition is satisfied (the so-called shock-domain) for flow without mass loss, also shrinks. Hence there is a possibility of mass loss induced shock instability too. Since shocks do not form for  $\xi = 0.0$  or  $e^- - e^+$  flow, purely  $e^- - e^+$  jet solutions are not found, although lepton dominated ( $0 < \xi < 1$ ) jets are possible. It must be noted that a purely  $e^- - e^+$  flow is essentially a flow described by fully ionized single species EoS. At temperatures  $T > 10^5$  the flow is likely to be fully ionized. A fully ionized flow comprised of similar particles can only be  $e^- - e^+$  flow. However, at the same time, an accretion disc from large distances to the horizon and made up of only the pair plasma is not likely to happen in nature. We compared  $e^- - e^+$  flow with other flows containing protons, only to show the stark contrast between a physically plausible flow and a flow which is not viable. Moreover, it is to be noted that in principle,  $\xi$  should be computed from physical processes self-consistently and not supplied as a parameter. In a given disc,  $\xi$  must be a function of the radial distance. We are working on this question and the results will be communicated elsewhere.

## ACKNOWLEDGMENT

CBS acknowledges the Visiting Students Programme in ARIES, where this work was initiated.

## REFERENCES

- Becker, P. A., Das, S., Le, T., 2008, ApJ, 677, L93  
 Blandford R.D., Payne D.G., 1982, MNRAS, 199, 883  
 Blumenthal, G. R. & Mathews, W. G. 1976, ApJ, 203, 714.  
 Burrows C.J. et al., ApJ, 1996, 473, 437  
 Chakrabarti S.K., ApJ, 1989, 347, 365  
 Chakrabarti, S. K., 1990, MNRAS, 243, 610.  
 Chakrabarti, S K., Titarchuk, L., 1995, ApJ, 455, 623.  
 Chakrabarti S.K., 1996, ApJ, 464, 664  
 Chakrabarti S.K., 1999, A&A, 351, 185



- Chakrabarti, S. K.; Das, S., 2004, MNRAS, 349, 649
- Chandrasekhar, S., 1938, An Introduction to the Study of Stellar Structure, Dover, New York.
- Chattopadhyay I., 2005, MNRAS, 356, 145.
- Chattopadhyay, I.; Das, S., 2007, New A, 12, 454
- Chattopadhyay, I., 2008, in Chakrabarti S. K., Majumdar A. S., eds, AIP Conf. Ser. Vol. 1053, Proc. 2nd Kolkata Conf. on Observational Evidence of Black Holes in the Universe and the Satellite Meeting on Black Holes Neutron Stars and Gamma-Ray Bursts. Am. Inst. Phys., New York, p. 353
- Chattopadhyay I., Ryu D., 2009, ApJ, 694, 492
- Chattopadhyay I., Chakrabarti S.K., 2011, Int. Journ. Mod. Phys. D, 20, 1597
- Das S., Chattopadhyay I., Nandi A., Chakrabarti S.K., 2001, A&A, 379, 683
- Das, S.; Chattopadhyay, I., 2008, New A, 13, 549.
- Fender, R. P., Gallo, E., Russell, D., 2010, MNRAS, 406, 1425.
- Fukue, J., 1987, PASJ, 39, 309
- Gallo, E., Fender, R. P., Pooley, G., G., 2003 MNRAS, 344, 60
- Giri, K., Chakrabarti, S. K., 2013, MNRAS, 430, 2826
- Junor W., Biretta J.A., Livio M., 1999, Nature, 401, 891
- Kumar R., Chattopadhyay I., 2013, MNRAS, 430, 386
- Liang, E. P. T., Thompson, K. A., 1980, ApJ, 240, 271L
- Lu, J. F., Gu, W. M., & Yuan, F. 1999, ApJ, 523, 340
- Mathews, W. G., 1971, ApJ, 165, 147
- Molteni, D., Lanzafame, G., Chakrabarti, S. K., 1994, ApJ, 425, 161
- Molteni, D., Ryu, D., Chakrabarti, S. K., 1996, ApJ, 470, 460
- Nandi, A., Debnath, D., Mandal, S., Chakrabarti, S. K., 2012, A&A, 542A, 56.
- Narayan, R., Kato, S., Honma, F., 1997, ApJ, 476, 49
- Novikov, I. D.; Thorne, K. S., 1973, in Dewitt B. S., Dewitt C., eds, Black Holes. Gordon & Breach, New York, p. 343
- Rushton, A., Spencer R., Fender, R., Pooley, G., 2010, A&A, 524, 29
- Shakura, N. I., Sunyaev, R. A., 1973, A&A, 24, 337S.
- Smith, D. M., Heindl, W. A., Marckwardt, C. B., Swank, J. H., 2001, ApJ, 554 L41.
- Smith, D. M., Heindl, W. A., Swank, J. H., 2002, ApJ, 569, 362.
- Smith, D. M., Dawson, D. M., Swank, J. H., 2007, ApJ, 669, 1138.

Punsly B., Coroniti F.V., 1990, ApJ, 350, 518

Paczynski, B. and Wiita, P.J., 1980, A&A, 88, 23.

Ryu, D., Chattopadhyay I., Choi E., 2006, ApJS, 166, 410

Singh C.B., Chakrabarti S.K., 2011a, MNRAS, 410, 2414

Singh C.B., Chakrabarti S.K., 2011b, Int. Journ. Mod. Phys. D, 20, 2507

Singh C.B., Chakrabarti S.K., 2012, MNRAS, 421, 1666

Synge, J. L., 1957, The Relativistic Gas, Amsterdam, North Holland.

Taub A.H., 1948, Phys. Rev., 74, 328